Pointing Model for Vehicular Quantum Communication Terminals Based on Line-of-Sight Attitude Measurement

Zihao Wang , Chao Peng , Tong Zhang, Xiang Liu, Qiang Wang, Shunfa Liu, Yuankang Wang, Yongmei Huang , and Dong He

Abstract—**Vehicular quantum communication terminals (VQCTs) are crucial for establishing global-scale quantum networks. High-precision line-of-sight (LOS) pointing is essential for fast and reliable acquisition in satellite-based quantum key distribution (QKD). The pointing accuracy of VQCTs is affected by attitude measurement errors, mechanical structure errors, and structural instability errors resulting from platform movement. By mounting attitude sensors on the LOS of VQCTs, we directly measure the LOS attitude. This completely eliminates the impact of mechanical structure errors and structural instability errors on pointing accuracy. Furthermore, we propose a line-of-pointing calibration method and a pointing model for VQCTs based on LOS attitude measurement. The pointing accuracy of this model is primarily reliant on the accuracy of attitude sensors. Two experiments were conducted to validate the effectiveness of our model. One is the star pointing experiment, comparing with the existing pointing model for VQCTs, our model significantly reduces the pointing errors by 93%, from 1296″ to 87.8″. This substantiates that our model eliminates mechanical structure errors and structural instability errors. Another is the successful acquisition of a quantum communication satellite, which demonstrates the feasibility of the proposed model for implementing the satellite-to-motion platform QKD and global-scale quantum networks.**

Index Terms—**Quantum communication, Vehicular quantum communication terminals(VQCT), line-of-sight (LOS) pointing, pointing model.**

Zihao Wang, Chao Peng, and Dong He are with the National Key Laboratory of Optical Field Manipulation Science and Technology, Chinese Academy of Sciences, Chengdu 610209, China, also with the Key Laboratory of Optical Engineering, Chinese Academy of Sciences, Chengdu 610209, China, also with the Institute of Optics and Electronics, Chinese Academy of Sciences, Chengdu 610209, China, also with the University of Chinese Academy of Sciences, Beijing 100049, China, and also with the School of Electronic, Electrical and Communication Engineering, University of Chinese Academy of Sciences, Beijing 101408, China (e-mail: wangzihao201@mails.ucas.ac.cn; 1638742360@qq.com; hedong@ioe.ac.cn).

Tong Zhang, Xiang Liu, Qiang Wang, Shunfa Liu, and Yuankang Wang are with the Key Laboratory of Optical Engineering, Chinese Academy of Sciences, Chengdu 610209, China, and also with the Institute of Optics and Electronics, Chinese Academy of Sciences, Chengdu 610209, China (e-mail: zt4832@163.com; lx061990@163.com; qiangwang@ioe.ac.cn; sfliu@ioe.ac.cn; lkzxing@foxmail.com).

Yongmei Huang is with the Key Laboratory of Optical Engineering, Chinese Academy of Sciences, Chengdu 610209, China, also with the Institute of Optics and Electronics, Chinese Academy of Sciences, Chengdu 610209, China, and also with the University of Chinese Academy of Sciences, Beijing 100049, China (e-mail: huangym@ioe.ac.cn).

Digital Object Identifier 10.1109/JPHOT.2024.3428932

I. INTRODUCTION

QUANTUM key distributions (QKDs) provide an efficient way to extend the information-theoretically secure key based on the fundamental principles of quantum mechanics. Since the proposal of the first QKD scheme and the table-top experiments in the 1980s [1], QKD has become the most active research field for practicality in quantum information science. To realize global-scale secure QKDs for practical use, many remarkable advancements have been made in the past decades, such as the demonstration of ground-fiber quantum communication networks in metropolitan areas in different countries [2], [3], [4], [5] and quantum communication experiments over 100 km free-space channels on the ground [6], [7], [8], [9], [10].

China launched the world's first quantum science satellite Micius, and a micro–nano quantum communications satellite, providing experimental conditions for testing the fundamentals of quantum communication in space. Recent implementations of satellite-based quantum communication experiments [11], [12], [13] have extended the feasible range of QKDs to approximately 4600 km [14], thereby demonstrating the feasibility for a future global-scale quantum communication network. To achieve this, mid-earth-orbit and high-earth-orbit quantum communication satellites are necessary. In order to establish a satellite-ground quantum communication link, the acquisition of quantum communication satellites by ground terminals is essential. Enhancing the line-of-sight (LOS) pointing accuracy of VQCTs is essential, as it improves acquisition probability and reduces acquisition time in communication [15]. And with the increase in satellite orbit altitude, the divergence angle of the beacon light is smaller, which requires VQCTs with higher pointing accuracy.

There are two methods to improve the VQCT pointing accuracy. The first is hardware correction through optimizing mechanical fabrication and assembly. Although effective, this method is expensive and difficult to implement. The second method is software correction. The pointing errors are corrected by analyzing the mechanical structure of terminals and developing a physical model or employing mathematical approaches such as numerical fitting. Compared with hardware correction, this method is more feasible and cost-effective to implement.

To facilitate global-scale QKD and broaden communication network coverage, existing approaches involve mounting

communication terminals on motion platforms such as ships and vehicles. Compared with stationary ground platforms, motion platforms are more complex and difficult to model, because these systems introduce additional attitude measurement errors and installation errors between the attitude sensor and the VQCT.

In response to these challenges, several researchers have proposed methods for correcting pointing errors of communication terminals on motion platforms. Wu et al. combined a global positioning system (GPS) with an inertial navigation system (INS) to achieve pointing of optical communication terminals (OCTs) on a motion platform [16]. He et al. modeled the installation errors of the INS and the self-errors of the OCTs separately to enhance the pointing accuracy [17]. Furthermore, Peng et al. developed parametric and non-parametric models of OCTs to improve their pointing accuracy [18], [19]. A common strategy in these methods is the installation of attitude sensors on the motion platform. Despite these advancements, existing models face limitations in fully correcting mechanical structure errors. For a VQCT, structural instability errors can also lead to a decrease in pointing accuracy. Gaps will be introduced in the manufacture and assembly of the terminals and it will change due to the dynamic nature of the motion platform, resulting in mechanical structural instability errors. This makes traditional pointing-error correction models less applicable [20].

To eliminate the influence of mechanical structure errors and structural instability errors on pointing accuracy, some studies installed attitude sensors on the LOS to directly measure the LOS attitude [21], [22]. This method avoids the influence of mechanical structure errors on guide angles calculation, and the pointing errors are mainly caused by attitude sensor installation errors and attitude measurement errors. Installation errors are constant and can be corrected by pre-calibration, therefore, the pointing accuracy is only affected by the attitude measurement errors. The Stratospheric Observatory for Infrared Astronomy (SOFIA) space telescope installed attitude sensors on the LOS [21]. Its LOS driven by spherical motors with three guide angles, indicating that their pointing model cannot be used on gimbal-type VQCTs. Hyosang Yoon et al. employed a star camera on a small ground station communication telescope to measure the LOS attitude [22]. However, their pointing model can only be used on stationary ground terminals. Previous studies have inadequately addressed the LOS attitude measurement–based pointing model for gimbal-type VQCTs. Thus, we propose a novel pointing model for VQCTs based on LOS attitude measurement and a line-of-pointing (LOP) calibration method. Initially, the LOP was calibrated using star tracking. This effectively corrects installation errors of the attitude sensor. Subsequently, the guide angles of the VQCT are calculated using the LOP and our pointing model. This strategy fundamentally eliminates the influence of mechanical structure errors and structural instability errors on pointing accuracy, thereby significantly improving the pointing accuracy of VQCTs. This advancement is particularly valuable in facilitating global-scale secure QKDs experiments. Significantly, quantum communication is a kind of free space
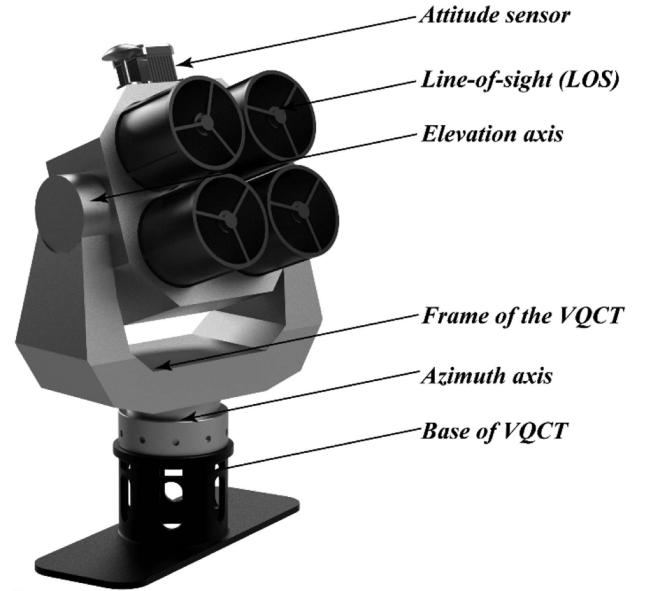

Fig. 1. Model of a vehicular quantum communication terminal.

laser communication. Although our pointing model was developed for VQCTs, it is also applicable to gimbal-type mounts with two perpendicular axes.

II. ANALYSIS OF THE POINTING ERRORS OF VQCTs

VQCT systems are complex systems integrating optics, electronics, and mechanical science. Fig. 1 shows the model of a VQCT. The system mainly comprises the LOS, encoders, a frame, and an attitude sensor as well as azimuth and elevation axes. Typically, the frame of a VQCT is gimbal-type. The rotation of the azimuth axis rotates the elevation axis, and the rotation of the elevation axis rotates the LOS. Encoders are used to measure the rotation angles of the azimuth and elevation axes. The attitude sensors measure the attitude of the LOS.

There are two methods for mounting the attitude sensor, one is mounted on the platform and the other is mounted on the LOS of the VQCT. Fig. 1 shows the method of mounting the attitude sensor on the LOS. In existing studies, attitude sensors are usually mounted on platforms. For an ideal VQCT, the azimuth axis is orthogonal to the elevation axis and the elevation axis is orthogonal to the LOS. Attitude sensors have no installation errors and no measurement errors. To establish a satellite-to-motion platform quantum communication link, the guide angles need to be calculated based on the satellite orbital prediction data and platform attitude. The azimuth and elevation axes are driven according to the guide angles, so that the LOS accurately points to the satellite. The ideal guide angles can be obtained from (1) and (2).

$$\begin{bmatrix} x_c \\ y_c \\ z_c \end{bmatrix} = \begin{bmatrix} \cos R_p & 0 & -\sin R_p \\ 0 & 1 & 0 \\ \sin R_p & 0 & \cos R_p \end{bmatrix} \begin{bmatrix} 1 & 0 & 0 \\ 0 & \cos P_p & \sin P_p \\ 0 & -\sin P_p & \cos P_p \end{bmatrix}$$
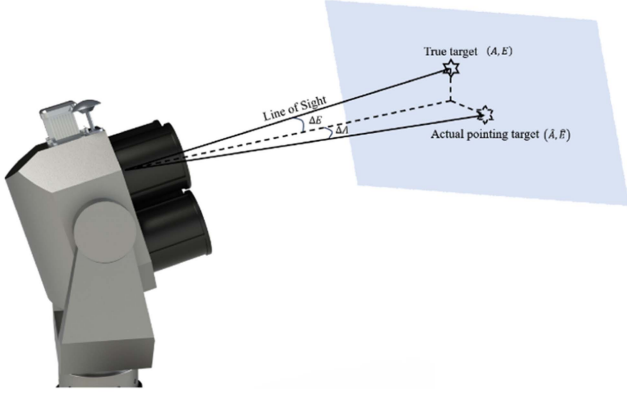
Fig. 2. Line-of-sight (LOS) pointing error.

Fig. 3. Schematic of line-of-pointing (LOP).

$$\begin{bmatrix} \cos H_p & -\sin H_p & 0 \\ \sin H_p & \cos H_p & 0 \\ 0 & 0 & 1 \end{bmatrix} \begin{bmatrix} \cos E_n \sin A_n \\ \cos E_n \cos A_n \\ \sin E_n \end{bmatrix} \quad (1)$$

where A_n and E_n represent azimuth and elevation angles of the target in the northeast celestial coordinate system, respectively, which can be calculated from the satellite orbit prediction data, the position of the platform and the current time; $(x_c, y_c, z_c)^T$ represents the vector between the target and the VQCT; and H_p, P_p, and R_p represent the heading, pitch, and roll angles of the platform, respectively.

$$A_c = \arctan\left(\frac{x_c}{y_c}\right)$$

$$E_c = \arcsin(z_c) \quad (2)$$

where A_c represents the guide angle of the azimuth axis and E_c represents the guide angle of the elevation axis. Equations (1) and (2) form the pointing model based on platform attitude measurements.

For an actual VQCT, errors will inevitably occur during manufacture and assembly. This makes the azimuth axis is non-orthogonal to the elevation axis, and the elevation axis is non-orthogonal to the LOS. Bearings have roundness errors. Encoders are unable to accurately measure rotation angles. These are mechanical structure errors in VQCTs. Furthermore, there are installation errors and attitude measurement errors. Installation errors can cause the coordinate systems of the attitude sensor and the VQCT to be misaligned. Because of these errors, the actual pointing angles deviates from the ideal pointing angles. ΔA and ΔE shown in Fig. 2 indicate the pointing errors of the azimuth and elevation axes, respectively, which are defined as

$$\begin{cases} \Delta A = \hat{A} - A \\ \Delta E = \hat{E} - E \end{cases} \quad (3)$$

where $\hat{A}$ and $\hat{E}$ represent the actual pointing angles of the of the azimuth and elevation axes, respectively, A and E represent the measured angles of the azimuth and elevation axis encoders, respectively, when the target is at the center of the field of view (FOV).
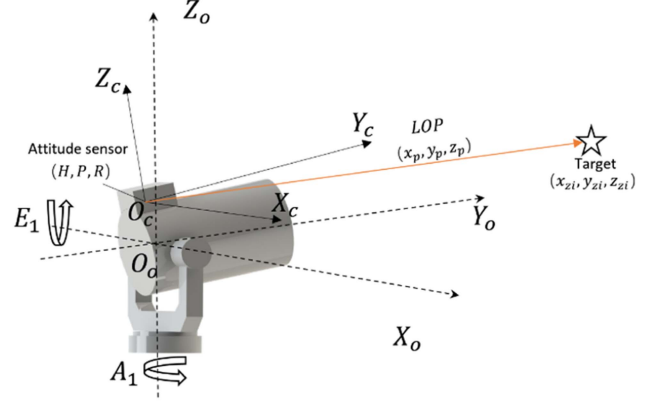
Mechanical structure errors will affect the calculation of the guide angles, and the platform movement will change the load, leading to variations in the mechanical structure of the VQCT. This introduces structural instability errors. Traditional models of pointing-error correction are inadequate for correcting mechanical structural instability errors. When the attitude sensor is mounted on the LOS, the guide angles are calculated directly using the LOS attitude. This eliminates the influence of mechanical structure errors and structural instability errors. Only attitude sensor measurement errors and installation errors remain as factors affecting pointing accuracy. However, for common gimbal-type VQCTs, there is no pointing model in the second mounting method. In order to fully utilize the advantages of this mounting method, it is necessary to study the pointing model for VQCTs based on LOS attitude measurement.

III. CALIBRATION OF LOP AND POINTING MODEL

Prior to detailing our pointing model, it is necessary to define the coordinate systems. Three coordinate systems are involved in the model: the northeast celestial coordinate system, the platform coordinate system, and the attitude sensor coordinate system. As shown in Fig. 3.

In the northeast celestial coordinate system, the X-axis points eastward from the location of the terminal, whereas the Y-axis and Z-axis point northward and skyward, respectively. When the encoder measurement of the VQCT is zero, the platform coordinate system $(O_O - X_O Y_O Z_O)$ defines the elevation axis of the VQCT as the X_o-axis, the azimuth axis as the Z_o-axis, and the Y_o-axis is defined according to the Cartesian coordinate system. The three axes of the attitude sensor coordinate system $(O_c - X_c Y_c Z_c)$ are its three measurement axes. When there are no installation errors, the X_c-axis aligns parallel to the X_o-axis of the platform coordinate system, the Y_c-axis aligns with the LOS direction, and the Z_c-axis is established by the Cartesian system. Additionally, the direction cosine matrix from the northeast celestial coordinate system to the attitude sensor coordinate system is defined as follows equation (4) shown at the bottom of the next page: where H, P, and R represent the heading angle, pitch angle, and roll angle measured by the attitude sensor, respectively.
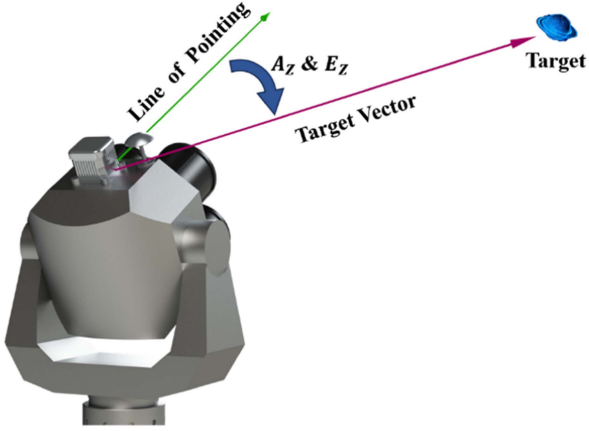
Fig. 4. Definition of the pointing model.

When the target is centered in the FOV, the LOS is pointing precisely at the target. At this moment, the position vector of the target in the attitude sensor coordinate system is a constant vector, which we define as the LOP. This vector was calibrated by manually tracking multiple known stars with the VQCT. The coarse calibration of the LOP using the i-th calibrated star as follows:

$$(x_i, y_i, z_i)^T = C_n^s (x_{zi}, y_{zi}, z_{zi})^T \qquad (5)$$

where $(x_i, y_i, z_i)^T$ represents the calculation of the LOP using the i-th star and $(x_{zi}, y_{zi}, z_{zi})^T$ represents the position vector of the i-th star in the northeast celestial coordinate system.

To mitigate the influence of random errors, the calculated values of multiple stars are averaged. This makes the LOP closer to the actual value. The calibration methodology is outlined as follows:

$$(x_p, y_p, z_p)^T = \frac{\sum_{i=1}^{n} (x_i, y_i, z_i)^T}{n} \qquad (6)$$

where $(x_p, y_p, z_p)^T$ represents the LOP of the calibration and n indicates the number of calibrated stars.

After the LOP is calibrated, we can define the pointing of the VQCT by aligning the LOP with the target vector through the rotation of the azimuth and elevation axes. This definition is illustrated in Fig. 4, and the target vector represents the vector of the target in the attitude sensor coordinate system. The aim of our pointing model is to compute the values of the azimuth and elevation axis encoders when the LOS is pointing precisely, defining these values as the guide angles (A_z, E_z).

At the current time, the conversion from the platform attitude to the LOS attitude is

$$C_{n_1}^{s_1} = C_X (E_1) C_Z (A_1) B_1 C_{n_o}^{s_o} \qquad (7)$$

where $C_{n_1}^{s_1}$ represents the direction cosine matrix from the northeast celestial coordinate system to the attitude sensor coordinate system at the current time; $C_{n_o}^{s_o}$ represents the direction cosine matrix from the northeast celestial coordinate systems to the platform coordinate systems; B_1 represents the current VQCT system error matrix; A_1 and E_1 represent current measurement values of the azimuth and elevation axes encoders, respectively; C_X represents the direction cosine matrix rotating around the X_o-axis; and C_Z represent the direction cosine matrix rotating around the Z_o-axis, respectively.

Furthermore, the conversion between the platform attitude and LOS attitudes when precisely pointing at the target as follows:

$$C_{n_z}^{s_z} = C_X (E_2) C_Z (A_2) B_2 C_{n_o}^{s_o} \qquad (8)$$

where $C_{n_z}^{s_z}$ represents the direction cosine matrix from the northeast celestial coordinate system to the attitude sensor coordinate system when precisely pointing at the target; A_2 and E_2 represent the guide angles of the azimuth and elevation axes, respectively and B_2 represents the VQCT system error matrix when pointing precisely.

In (7) and (8) the direction cosine matrix from the northeast celestial coordinate system to the platform coordinate system $C_{n_o}^{s_o}$ is the same. The combination of (7) and (8) is stated as follows:

$$[C_X (E_1) C_Z (A_1) B_1]^{-1} C_{n_1}^{s_1} = [C_X (E_2) C_Z (A_2) B_2]^{-1} C_{n_z}^{s_z} \qquad (9)$$

where B_1 and B_2 are related to mechanical structure errors and installation errors, both of which are small errors [23], so (9) can be approximated as

$$[C_X (E_1) C_Z (A_1)]^{-1} C_{n_1}^{s_1} = [C_X (E_z) C_Z (A_z)]^{-1} C_{n_z}^{s_z} \qquad (10)$$

where A_z and E_z represent the approximate guide angles of the azimuth and elevation axes, respectively.

During the pointing process, using (10), the approximate guide angles can be calculated to drive the azimuth and elevation axes. This will make the LOP gradually closer to the target vector. When the two vectors coincide, in (9), $B_1 = B_2$ and the approximate guide angles are the same as the actual guide angles. Therefore, using the approximate guide angles, in the end, can make the LOS precisely point to the target. For computational convenience, (10) will be used to solve for the guide angles.

As $C_{n_z}^{s_z}$ is unknown, it is difficult to solve for the guide angles directly using (10), multiplying both sides of (10) by the position vector of the target in the northeast celestial coordinate system $(x_z, y_z, z_z)^T$ yields

$$[C_X (E_1) C_Z (A_1)]^{-1} C_{n_1}^{s_1} (x_z, y_z, z_z)^T$$
$$= [C_X (E_z) C_Z (A_z)]^{-1} C_{n_z}^{s_z} (x_z, y_z, z_z)^T \qquad (11)$$

$$C_n^s = \begin{bmatrix} \cos H \cos R + \sin H \sin P \sin R & -\sin H \cos R + \cos H \sin P \sin R & -\cos P \sin R \\ \sin H \cos P & \cos H \cos P & \sin P \\ \cos H \sin R - \sin H \sin P \cos R & -\sin H \sin R - \cos H \sin P \cos R & \cos P \cos R \end{bmatrix} \qquad (4)$$

Combining (5), (6) and (11) yields:

$$[C_X(E_1) C_Z(A_1)]^{-1} C_{n_1}^{s_1} (x_z, y_z, z_z)^T$$
$$= [C_X(E_z) C_Z(A_z)]^{-1} (x_p, y_p, z_p)^T \quad (12)$$

The value on the left-hand side in (12) is known and can be equated to $[T_1, T_2, T_3]$, as expressed in (13).

$$[C_X(E_1) C_Z(A_1)]^{-1} C_{n_1}^{s_1} (x_z, y_z, z_z)^T = [T_1, T_2, T_3] \quad (13)$$

The right-hand side of (12) can be expanded as expressed in (14).

$$[C_X(E_z) C_Z(A_z)]^{-1} (x_p, y_p, z_p)^T$$
$$= [x_p \cos A_z + y_p \cos E_z \sin A_z - z_p \sin E_z \sin A_z$$
$$- x_p \sin A_z + y_p \cos E_z \cos A_z - z_p \sin E_z \cos A_z$$
$$y_p \sin E_z + z_p \cos E_z] \quad (14)$$

From (12), (13) and (14) we obtain the following three equations

$$T_1 = x_p \cos A_z + y_p \cos E_z \sin A_z - z_p \sin E_z \sin A_z \quad (15)$$

$$T_2 = -x_p \sin A_z + y_p \cos E_z \cos A_z - z_p \sin E_z \cos A_z \quad (16)$$

$$T_3 = y_p \sin E_z + z_p \cos E_z \quad (17)$$

We can calculate the elevation guide angle using (17) as

$$E_z = \arcsin\left[\frac{2T_3 y_p + \sqrt{(2T_3 y_p)^2 - 4(y_p^2 + z_p^2)(T_3^2 - z_p^2)}}{2(y_p^2 + z_p^2)}\right] \quad (18)$$

Combining (15) and (16), extracting $\sin A_z$ and $\cos A_z$ to the left-hand side of the equation and making them equal to SA and CA yields

$$\begin{bmatrix} SA \\ CA \end{bmatrix} = \begin{bmatrix} \sin A_z \\ \cos A_z \end{bmatrix}$$
$$= \begin{bmatrix} y_p \cos E_z - z_p \sin E_z & x_p \\ -x_p & y_p \cos E_z - z_p \sin E_z \end{bmatrix}^{-1} \begin{bmatrix} T_1 \\ T_2 \end{bmatrix} \quad (19)$$

The azimuth guide angle is calculated as

$$A_z = \arctan\left(\frac{SA}{CA}\right) \quad (20)$$

Our pointing model is formed by (13) to (20).

The LOS pointing process is depicted in Fig. 5. In VQCT system, the position of the target in the northeast celestial coordinate system can be calculated from the target position in the J2000 coordinate system, the latitude and longitude of the platform, and the current time. The guide angles were then calculated using the target position in the northeast celestial coordinate system, the current encoder measurements, and the LOS attitude. The azimuth and elevation axes begin to rotate according to the guide angles. During the platform movement, the target position, LOS attitude, and encoder values of the VQCT are updated in real time, and real-time guide angles can be calculated. Until
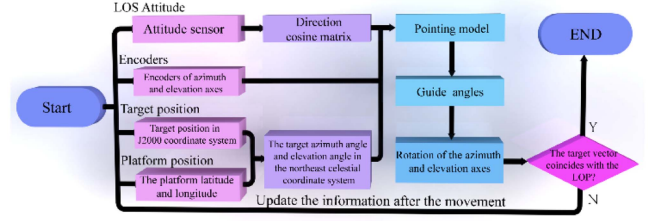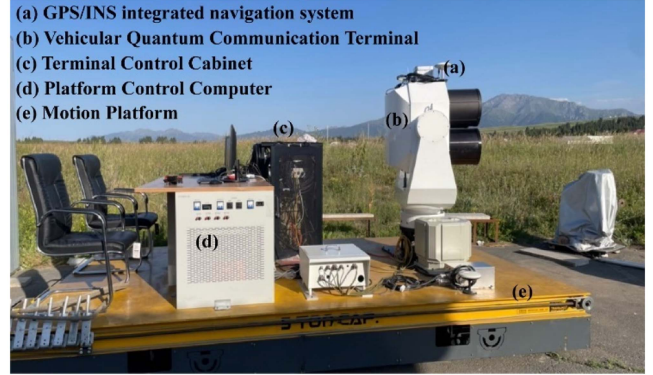

Fig. 5. Pointing process of the VQCT.

(a) GPS/INS integrated navigation system
(b) Vehicular Quantum Communication Terminal
(c) Terminal Control Cabinet
(d) Platform Control Computer
(e) Motion Platform

Fig. 6. VQCT system used in experiment.

TABLE I
DETECTOR PARAMETERS

Categories	Parameters
Field of View	$0.20° \times 0.11°$
Resolution	2048×1088
Pixel Size	5.5×5.5 μm
Frame Rate	20 Hz

the target vector coincides with the LOP, the pointing process is complete.

IV. STAR POINTING AND SATELLITE ACQUISITION EXPERIMENTS WITH A VQCT SYSTEM

The effectiveness of our pointing model is demonstrated through star pointing experiments and quantum communication satellite acquisition experiments. As shown in Fig. 6, a VQCT system was designed and constructed to conduct these experiments. This system is approximately 3 tons in weight, 2.5 m in height, 4 m in length, and 3 m in width. The azimuth axis of the VQCT has a rotation angle range of 0°–360°, the elevation axis has a rotation angle range of approximately −10° to 80°. Maximum tracking speed for both axes is 5°/s. Encoders for the azimuth and elevation axes have a resolution of 24 bits, which is equivalent to $0.077''$. Camera in the quantum communication terminal has a field of view of $0.20° \times 0.11°$, resolution of 2048×1088, and pixel size of 5.5×5.5 μm. Frame rate: 20 Hz. Detector parameters are listed in Table I. This VQCT system is

equipped with four telescopes, and only one telescope needs to be used as a calibration baseline in the experiment. A GPS/INS integrated navigation system, mounted on the LOS as an attitude sensor, is used to measure the LOS attitude in the northeast celestial coordinate system. The attitude measurement errors are 0.05° (1σ) for heading angles and 0.01° (1σ) for pitch and roll angles. In the results of experiments, the pointing errors of azimuth and elevation axes are expressed as root–mean–square errors (RMSEs), and the total pointing error calculated using the following equation:

$$\delta = \sqrt{\delta_A^2 + \delta_E^2} \qquad (21)$$

where δ(RMSE) represents the total pointing error; δ_A (RMSE)represents the azimuth pointing error; and δ_E(RMSE) represents the elevation pointing error.

Due to limitations at the experimental site, our platform mainly rotates in place. This approach enables the VQCT to be realized with azimuth angle variation in the range of 0°–360°, pitch angle variation in the range of −0.25°–0.45°, and roll angle variation in the range of 0°–1.2°. During the star pointing experiments, we first manually guided the stars into the FOV. The closed-loop feature of the VQCT was then used to maintain the star at the FOV center. Simultaneously, the VQCT automatically recorded the azimuth and elevation angles of the target in the northeast celestial coordinate system, the attitude angles of the GPS/INS integrated navigation system, and the measurements of the azimuth and elevation axis encoders. Furthermore, the LOP was calibration using recorded data. Afterwards, the platform changes multiple attitudes, and makes the VQCT point to the stars using our model and control system. During the experiment, the off-target amounts of the star in the FOV were recorded and the pointing errors were calculated as

$$\xi_A = \varepsilon_A \cdot eqwtA / \cos(E_1) \qquad (22)$$

$$\xi_E = \varepsilon_E \cdot eqwtE \qquad (23)$$

where ξ_A and ξ_E represent pointing errors in azimuth and elevation, respectively; ε_A and ε_E represent the off-target amounts of the azimuth and elevation in the FOV, respectively; $eqwtA$ and $eqwtE$ represent the rotation angles of the azimuth and elevation axes corresponding to a single pixel in the FOV, respectively.

In addition, a comparative experiment was conducted with the attitude sensor mounted on the platform. Point to stars using a pointing model based on platform attitude measurements formed by (1) and (2). Change multiple attitudes and record off-target amounts. This comparison can effectively show the advantages of the pointing model based on the LOS attitude measurement in avoiding the mechanical structure error and the structural instability error.

Fig. 7 presents the azimuth and elevation angles of stars for our experiment. As illustrated in Fig. 8, when the GPS/INS integrated navigation system is mounted on the platform, and points to stars using the pointing model based on platform attitude measurement, the total pointing error is 1269″. This is a poor pointing accuracy, which is caused by the significant errors in its manufacturing and assembly of this VQCT system. The
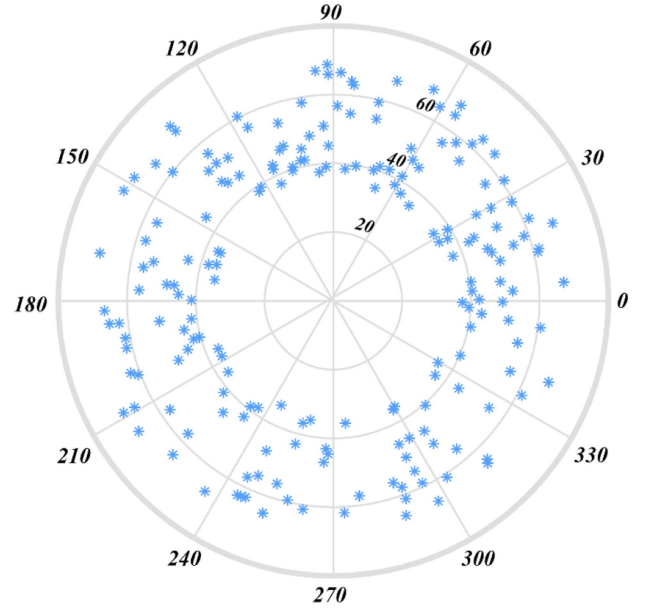

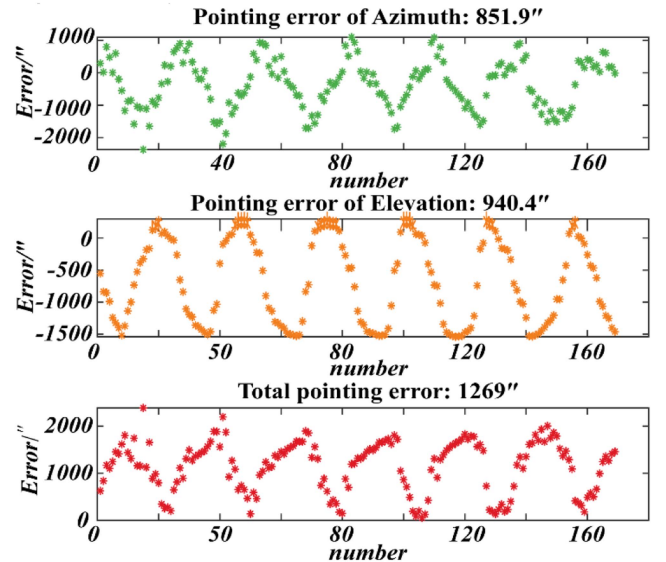Fig. 7. Polar diagram of the target stars in the experiment.

Fig. 8. Pointing errors in the pointing model based on platform attitude measurements.

movement of the platform also introduces structural instability errors that make the pointing error appear as a very regular curve.

Fig. 9 displays the experimental results of our pointing model. The total pointing error is 87.8″. Since our pointing model is not affected by the mechanical structure error and structural instability error in the calculation, it can effectively improve the pointing accuracy. Comparing Figs. 8 and 9, the total pointing error has been substantially reduced from 1269″ to 87.8″, a decrease of approximately 93%. The pointing error of our pointing model is only related to measurement errors of the attitude sensor. This accuracy does not represent the upper and lower bounds of our
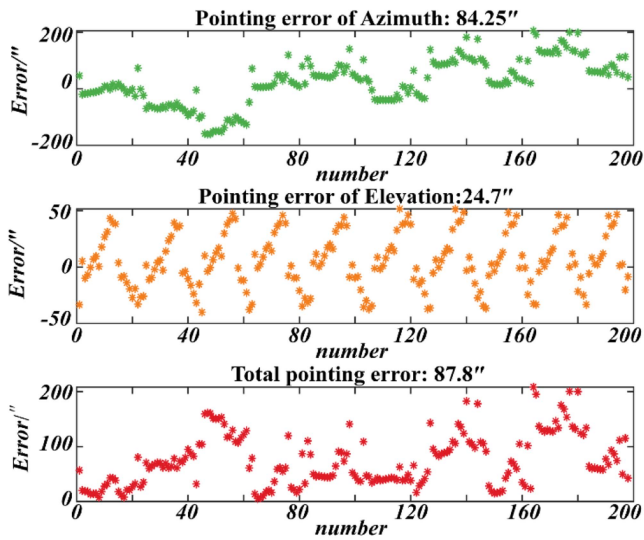
Fig. 9. Pointing errors in the pointing model based on platform attitude measurements.
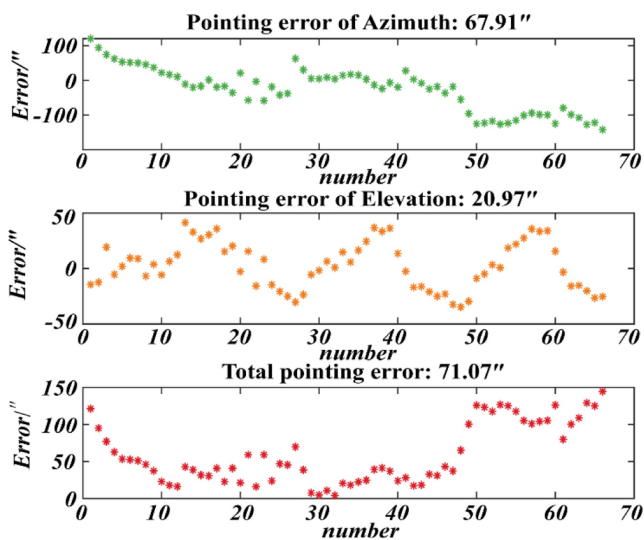

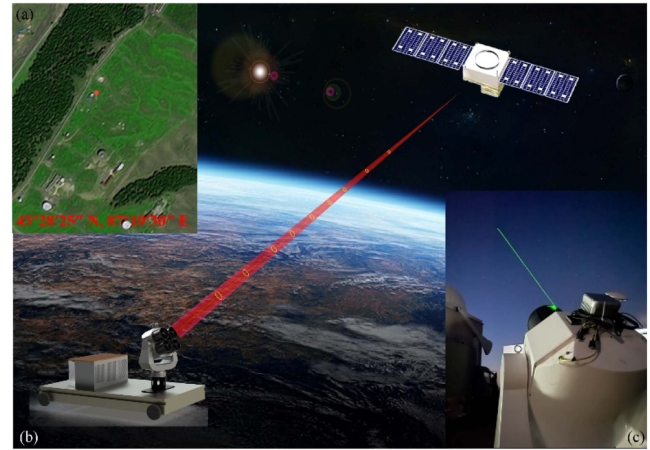Fig. 10. Plot of pointing errors for repeated experiments.

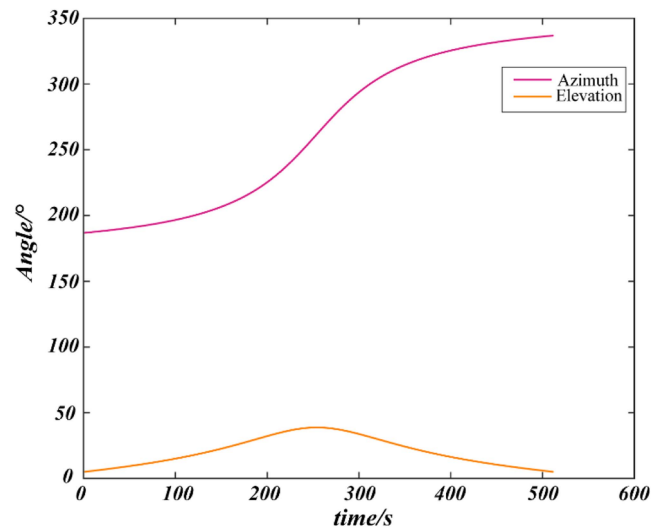Fig. 11. Overview of the quantum communications satellite acquisition and tracking experiment.

Fig. 12. Jinan-1 satellite orbit data.

TABLE II
OVERVIEW OF SATELLITE ACQUISITION AND TRACKING EXPERIMENTS

Categories	Parameters
Elevation of entry	5.0581°
Maximum pitch angle	38.7528°
Elevation of departure	5.0085°
Angle of acquisition	A:226.3482°, E:32.5818°
Initial pointing error	80.94"

pointing model, and higher pointing accuracy can be obtained if a higher accuracy attitude sensor is used.

We repeated the experiment with the pointing model based on LOS attitude measurements. Results are illustrated in Fig. 10. The total pointing error is 71.07″. From Figs. 9 and 10, it can be seen that the pointing accuracy of the VQCT is similar in both experiments, which further illustrates the validity and reliability of our model.

Additionally, we conducted multiple acquisition and tracking experiments of the quantum communication satellite Jinan-1 in Xinjiang Province. The overview of the experiment is illustrated in Fig. 11. During these experiments, the orbit data of the satellite was input into the VQCT, and the uplink beacon was activated. The VQCT then pointed and gazed to the satellite to acquire of the satellite downlink beacon. Once the downlink

beacon light enters the FOV, the closed-loop functionality of the VQCT was utilized to rapidly centralize the beacon light in the FOV. This indicates the successful acquisition of a quantum communication satellite and the establishment of a quantum communication link.

The geographic location (43°28′25″ N, 87°10′30″ E) of our experiment is illustrated in Fig. 11(a). We successfully captured

satellite downlink beacons several times. Table II shows a representative quantum communication satellite acquisition result, with all times denoted in UTC. The satellite was entered at 16:40:01, and the VQCT was pointed according to the orbit data. As to the satellite rises from the horizon at a long distance, the beacon light is difficult to acquire, and as the satellite moves, the downlink beacon light is successfully acquired and tracked at 16:43:22. The azimuth and elevation angles of the VQCT at the time of acquisition were 226.3428° and 32.5818°, respectively. The initial pointing error based on the off-target amounts of downlink beacons just entering the FOV was 80.94″. Moreover, Fig. 12 displays the orbital data of the satellite during the experiment.

V. CONCLUSION

Numerous factors affect the pointing accuracy of VQCT systems, including mechanical structure errors and structural instability errors. Mechanical structure errors occur during manufacturing and assembly, and structural instability errors are caused by platform motion. These errors make existing pointing models less applicable. Therefore, we propose to mount the attitude sensor on the LOS and introduce a pointing model for VQCT based on LOS attitude measurement. This model eliminates the influence of mechanical structure errors and structural instability errors on pointing accuracy.

Our model has been validated through star pointing experiments and quantum communication satellite acquisition experiments. Compared to the pointing model based on the platform attitude measurements, our model significantly reduces the pointing error by 93%, from 1296″ to 87.8″. This reduction demonstrates the effectiveness of our model in eliminating the influence of mechanical structure errors and structural instability errors on the VQCT pointing accuracy. In the quantum communication satellite acquisition and tracking experiment, our pointing model achieves the acquisition of quantum communication satellites on vehicle systems. It lays the foundation for satellite-to-motion platform QKD and the establishment of a global-scale quantum network. The pointing errors in our model is solely depends on the accuracy of the attitude sensor. To achieve higher pointing accuracy, an attitude sensor with higher measurement accuracy can be used.

In the future, we plan to further improve the pointing accuracy by using VQCTs to compensate for the attitude sensor measurement errors.

REFERENCES

[1] C. H. Bennett, F. Bessette, G. Brassard, L. Salvail, and J. Smolin, "Experimental quantum cryptography," *J. Cryptology*, vol. 5, pp. 3–28, 1992.

[2] H. Takesue et al., "Quantum key distribution over a 40-dB channel loss using superconducting single-photon detectors," *Nature Photon.*, vol. 1, no. 6, pp. 343–348, 2007.

[3] D. Stucki et al., "High rate, long-distance quantum key distribution over 250 km of ultra low loss fibres," *New J. Phys.*, vol. 11, no. 7, 2009, Art. no. 075003.

[4] Y. Liu et al., "Decoy-state quantum key distribution with polarized photons over 200 km," *Opt. Exp.*, vol. 18, no. 8, pp. 8587–8594, 2010.

[5] C.-Q. Hu et al., "Transmission of photonic polarization states through 55-m water: Towards air-to-sea quantum communication," *Photon. Res.*, vol. 7, no. 8, pp. A40–A44, 2019, doi: 10.1364/PRJ.7.000A40.

[6] R. Ursin et al., "Entanglement-based quantum communication over 144 km," *Nature Phys.*, vol. 3, no. 7, pp. 481–486, 2007.

[7] T. Schmitt-Manderbach et al., "Experimental demonstration of free-space decoy-state quantum key distribution over 144 km," *Phys. Rev. Lett.*, vol. 98, no. 1, 2007, Art. no. 010504.

[8] A. Fedrizzi et al., "High-fidelity transmission of entanglement over a high-loss free-space channel," *Nature Phys.*, vol. 5, no. 6, pp. 389–392, 2009.

[9] J. Yin et al., "Quantum teleportation and entanglement distribution over 100-kilometre free-space channels," *Nature*, vol. 488, no. 7410, pp. 185–188, 2012.

[10] X.-S. Ma et al., "Quantum teleportation over 143 kilometres using active feed-forward," *Nature*, vol. 489, no. 7415, pp. 269–273, 2012.

[11] W. Li et al., "High-rate quantum key distribution exploiting integrated photonics and multi-pixel superconducting nanowire detectors," in *Proc. IEEE Conf. Lasers Electro-Opt.*, 2023, pp. 1–2.

[12] J. Yin et al., "Satellite-based entanglement distribution over 1200 kilometers," *Science*, vol. 356, no. 6343, pp. 1140–1144, 2017.

[13] S.-K. Liao et al., "Satellite-to-ground quantum key distribution," *Nature*, vol. 549, no. 7670, pp. 43–47, 2017.

[14] Y.-A. Chen et al., "An integrated space-to-ground quantum communication network over 4,600 kilometres," *Nature*, vol. 589, no. 7841, pp. 214–219, 2021.

[15] S. Wu, L. Tan, S. Yu, and J. Ma, "Analysis and correction of axis error in periscope-type optical communication terminals," *Opt. Laser Technol.*, vol. 46, pp. 127–133, 2013.

[16] R. Wu, X. Zhao, Y. Liu, and Y. Song, "Initial pointing technology of line of sight and its experimental testing in dynamic laser communication system," *IEEE Photon. J.*, vol. 11, no. 2, Apr. 2019, Art. no. 7903008.

[17] D. He et al., "Shipborne acquisition, tracking, and pointing experimental verifications towards satellite-to-sea laser communication," *Appl. Sci.*, vol. 9, no. 18, 2019, Art. no. 3940.

[18] C. Peng et al., "Modeling and correction of pointing errors in gimbals-type optical communication terminals on motion platforms," *IEEE Photon. J.*, vol. 13, no. 3, Jun. 2021, Art. no. 6600915.

[19] C. Peng et al., "Pointing-error correction of optical communication terminals on motion platforms based on a K-nearest neighbor algorithm," *IEEE Photon. J.*, vol. 14, no. 6, Dec. 2022, Art. no. 6663807.

[20] Z. Jinyu, "Error analysis and correction technology for photoelectricity telescope," Changchun Institute of Optics Fine Mechanics and Physics Chinese Academy of Sciences, 2005.

[21] R. Yee and F. L. Robbins Jr, "Airborne blind pointer," *Proc. SPIE*, vol. 3351, pp. 32–39, 1998.

[22] H. Yoon, K. Riesing, and K. Cahoy, "Satellite tracking system using amateur telescope and star camera for portable optical ground station," 2016.

[23] H. Hong, X. Zhou, Z. Zhang, and D. Fan, "Modeling and calibration of pointing errors using a semi-parametric regression method with applications in inertially stabilized platforms," *Proc. Inst. Mech. Engineers, Part B: J. Eng. Manufacture*, vol. 227, no. 10, pp. 1492–1503, 2013.